Provided for non-commercial research and education use.
Not for reproduction, distribution or commercial use.

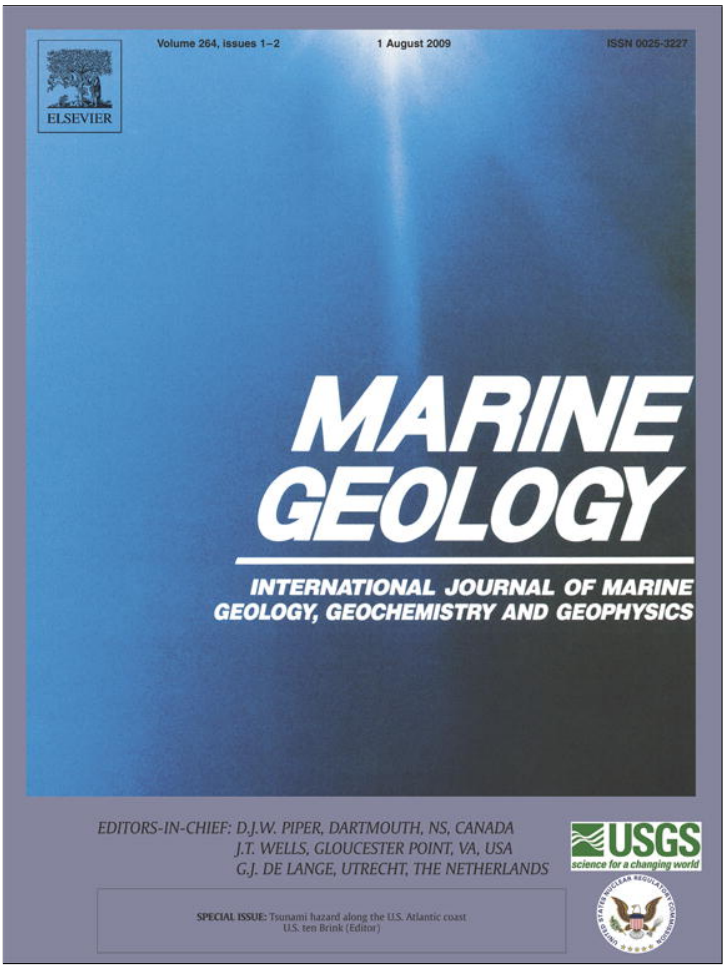

This article appeared in a journal published by Elsevier. The attached copy is furnished to the author for internal non-commercial research and education use, including for instruction at the authors institution and sharing with colleagues.

Other uses, including reproduction and distribution, or selling or licensing copies, or posting to personal, institutional or third party websites are prohibited.

In most cases authors are permitted to post their version of the article (e.g. in Word or Tex form) to their personal website or institutional repository. Authors requiring further information regarding Elsevier's archiving and manuscript policies are encouraged to visit:

http://www.elsevier.com/copyright

Author's personal copy

Marine Geology 264 (2009) 98–108

Contents lists available at ScienceDirect

Marine Geology

journal homepage: www.elsevier.com/locate/margeo

Assessment of source probabilities for potential tsunamis affecting the U.S. Atlantic coast

Eric L. Geist *, Tom Parsons

U.S. Geological Survey, 345 Middlefield Rd., MS 999, Menlo Park, CA 94025, USA

ARTICLE INFO

Article history:
Received 16 February 2008
Received in revised form 18 July 2008
Accepted 6 August 2008

Keywords:
tsunami
probability
Atlantic Ocean
earthquake
landslide
hazard

ABSTRACT

Estimating the likelihood of tsunamis occurring along the U.S. Atlantic coast critically depends on knowledge of tsunami source probability. We review available information on both earthquake and landslide probabilities from potential sources that could generate local and transoceanic tsunamis. Estimating source probability includes defining both size and recurrence distributions for earthquakes and landslides. For the former distribution, source sizes are often distributed according to a truncated or tapered power–law relationship. For the latter distribution, sources are often assumed to occur in time according to a Poisson process, simplifying the way tsunami probabilities from individual sources can be aggregated. For the U.S. Atlantic coast, earthquake tsunami sources primarily occur at transoceanic distances along plate boundary faults. Probabilities for these sources are constrained from previous statistical studies of global seismicity for similar plate boundary types. In contrast, there is presently little information constraining landslide probabilities that may generate local tsunamis. Though there is significant uncertainty in tsunami source probabilities for the Atlantic, results from this study yield a comparative analysis of tsunami source recurrence rates that can form the basis for future probabilistic analyses.

Published by Elsevier B.V.

1. Introduction

A probabilistic approach is the best method to fully assess the hazard posed by tsunamis for a wide range of sizes. Tsunami probability is calculated from the distribution of earthquake or landslide sizes and the recurrence distribution of events in time. For coastal locations that have a long record of tsunamis, the size distribution is best described as a power–law (Burroughs and Tebbens, 2005), similar to the distribution of many other natural hazards such as earthquakes, landslides, and forest fires (e.g., Hergarten, 2002). In oceans such as the Pacific, tsunamigenic earthquakes from many different subduction zones influence tsunami probability at any given location because of the slowly-attenuating nature of tsunamis during propagation over long distances. In the Atlantic Ocean, however, the number of tsunami source zones is much more limited. As such, it is unclear whether the size distribution and recurrence distribution of tsunamis along the U.S. Atlantic coast is similar in functional form to sites around the Pacific.

Because tsunami records along the Atlantic coast are sparse in both space and time, empirical approaches to define tsunami probabilities from, for example, tsunami catalogs are of limited use. In this study, we first describe the general framework for a computational approach to Probabilistic Tsunami Hazard Analysis (PTHA). We then focus on different approaches for determining source probabilities for both landslides and earthquakes and for both locally-generated and transoceanic tsunamis. Like tsunamis themselves, source probabilities are described by size and recurrence distributions. The applicable size parameter in this case is the primary source parameter for generating tsunamis. For earthquakes, this parameter is seismic moment m, where moment magnitude M_w is given by $M_w = (2/3)\,(\log(m) - 9.05)$, with secondary influence on tsunami generation from earthquake source depth and focal mechanism (e.g., Ward, 1980; Okal, 1988). For landslides, the primary source parameter is volume V, although landslide thickness (which may not scale with volume), landslide speed, and submergence depth also significantly affects tsunami generation (e.g., Harbitz, 1992; Lynett and Liu, 2002; Murty, 2003; Fritz et al., 2004; Grilli and Watts, 2005; Liu et al., 2005; Løvholt et al., 2005; Fritz, 2006; Geist et al., 2009-this issue). Secondary parameters such as these can be determined from mobility analysis (e.g., Locat et al., 2009-this issue) or scaling relations, with their attendant uncertainty included directly into probabilistic calculations. In terms of the recurrence distribution, a common assumption is that the recurrence rate is independent of time and that inter-event times are uncorrelated because source zones are physically uncorrelated. In statistical terms, this is the temporal description of a Poisson process. In addition to assessing the size distribution for tsunami sources, we briefly review evidence to determine whether earthquakes and landslides behave as a Poisson process.

* Corresponding author. Tel.: +1 650 329 5457; fax: +1 650 329 5411.
E-mail address: egeist@usgs.gov (E.L. Geist).

0025-3227/$ – see front matter. Published by Elsevier B.V.
doi:10.1016/j.margeo.2008.08.005

Author's personal copy

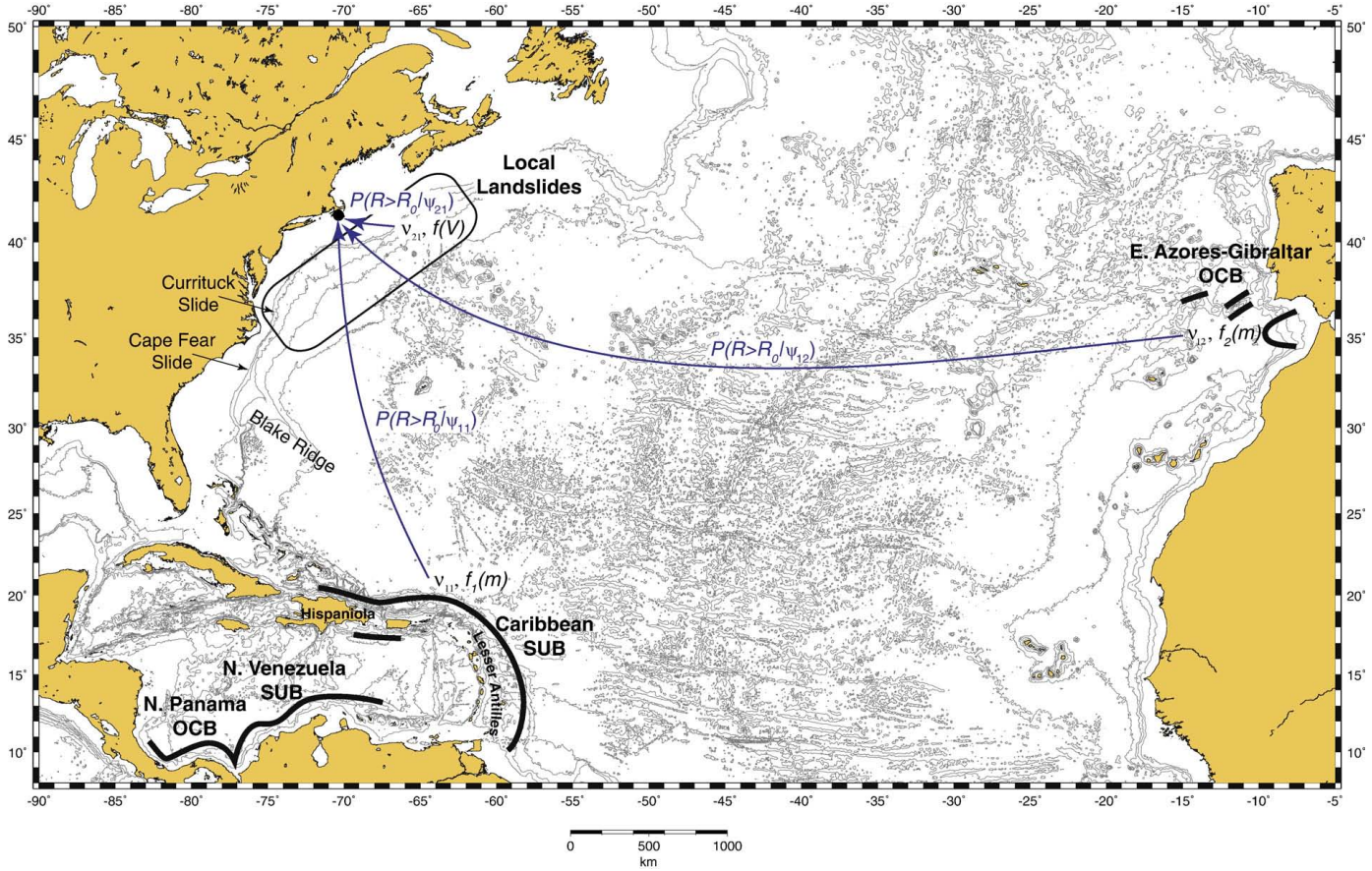

Fig. 1. Schematic diagram of how tsunami probabilities is aggregated for a particular coastal location. Two types of sources (earthquakes and landslides: index $i = 1, 2$, respectively) are indicated. Each source is associated with a particular zonation scheme (index j). For landslides in this example, zonation is geographic, whereas for earthquakes the zonation is according to plate boundary type and location.

Author's personal copy

2. General framework of Probabilistic Tsunami Hazard Analysis (PTHA)

Probabilistic Tsunami Hazard Analysis (PTHA) (Geist and Parsons, 2006; Geist et al., 2009) is directly derived from probabilistic seismic hazard analysis (PSHA) (Senior Seismic Hazard Analysis Committee (SSHAC), 1997) with some significant modifications. Like PSHA, there are essentially three steps involved: (1) define the source parameters, including source probabilities for all relevant tsunami sources; (2) calculate wave heights and other hydrodynamic parameters for each source; and (3) aggregate the results to determine the tsunami hazard curve for a particular coastal site or the probabilistic inundation map for a particular coastal region. The source parameters specified in step (1) are those that directly relate to the volume of water displaced during a submarine earthquake or landslide. These include primary geologic parameters such as the moment magnitude (M_w) of the earthquake or volume (V) of the landslide, as well as secondary source parameters such as landslide thickness and speed and the water depth above the source. Unlike PSHA, sources at much larger distances are considered for PTHA, because of the slowly-attenuating propagation characteristics of tsunami waves. As a notable example of the far-traveled nature of tsunamis, the M_w 9.2 2004 Sumatra–Andaman earthquake along the Sunda subduction zone in the Indian Ocean resulted in small tsunami amplitudes recorded along the U.S. Atlantic coast (Titov et al., 2005).

Step (2) in PTHA can be implemented using numerical models and the known bathymetry of the world's ocean. For PSHA, in contrast, step (2) linking the source and site is often implemented using empirical and stochastic attenuation relationships (and their attendant uncertainty). Because the horizontal dimensions of seafloor deformation near the tsunami source are typically much greater than the water depth, tsunami propagation is modeled using the shallow-water or long-wave equations (Liu, 2009). For landslide tsunamis, however, high-order hydrodynamic equations that incorporate dispersion and non-linearity are often necessary (Lynett and Liu, 2002). These equations can be implemented using finite-difference or finite-element methods and accurately simulate many aspects of wave propagation, such as focusing, dispersion, shoaling amplification, etc. As tsunami waves approach shore and inundate coastal regions, the hydrodynamics become considerably more complex (Imamura, 2009; Yeh, 2009). Inundation models need to account for non-linearity in wave propagation, bottom friction, turbulence, and other site specific factors. The size of a tsunami at a particular coastal location can be measured by the amplitude (amp) of the offshore wave (determined from propagation models) or more accurately, by runup (R), which is the water level height above ambient sea level at the point of farthest onshore inundation (determined from inundation models).

To calculate the probability that a tsunami with runup greater than a specified minimum value (R_0) will occur at a coastal location for an exposure time T (step 3 in PTHA), it is first necessary to know the distribution of recurrence times. Most often, an exponential distribution that is associated with a Poisson process is assumed such that

$$P(R > R_0, T) = 1 - e^{-\lambda T}, \tag{1}$$

where P is the probability that one or more tsunamis with $R > R_0$ will occur in time T, and λ is the rate at which these tsunamis occur. To test whether or not tsunamis are best described by a Poisson process, Geist and Parsons (2008) examine the distribution of inter-event times from the National Geophysical Data Center (NGDC) global tsunami catalog (http://www.ngdc.noaa.gov/hazard/tsu_db.shtml). Results indicate that the observed distribution deviates from that expected for a Poisson process at short recurrence times, indicative of a temporal clustering effect that is also observed for earthquake inter-event times (Corral, 2004). Therefore, the hazard rate increases slightly immediately after an event, but is otherwise that of a Poisson process.

The equation to calculate the Poisson rate (λ) at which tsunamis will exceed a certain runup (R_0) at a coastal location from all relevant sources is

$$\lambda(R > R_0) = \sum_{\text{type}=i} \sum_{\text{zone}=j} \nu_{ij} \int P\left(R > R_0 \,|\, \psi_{ij}\right) f\left(\psi_{ij}\right) \mathrm{d}\psi, \tag{2}$$

where the index i refers to the type of tsunami source (e.g., $i=1$ for earthquakes, $i=2$ for landslides, etc.), index j identifies the zone in which that source occurs (according to some particular zonation scheme), $\nu_{i,j}$ the mean rate for each source (i,j) where $R > R_0$, $\psi_{i,j}$ is the tsunami source parameters for source (i,j) (Ward, 2001), f_ψ is the probability distribution for tsunami source parameters, and $P(R > R_0|\psi_{ij})$ is the probability that runup will exceed R_0 at the coastal location for a given source parameter or set of source parameters (Geist et al., 2009). The propagation distance and other propagation factors such as ray path are implicitly included in the term $P(R > R_0|\psi_{ij})$ since this term is computed by numerical propagation models (step 2). In the absence of any uncertainty, this term is simply $1 - H(R)$ for a given set of source parameters, where H is the Heaviside step function. For earthquakes, the primary source parameter is seismic moment m such that $f(\psi_{1j})$ is the size distribution $f(m_j)$, whereas for landslides it is volume V such that $f(\psi_{2j}) = f(V_j)$. Other source parameters can be included in the probabilistic analysis through the f_ψ term, although size (i.e., seismic moment or volume) distributions are best constrained by the available data. Secondary parameters such as slip distribution (earthquakes) and landslide time history can alternatively be included as sources of uncertainty in the $P(R > R_0|\psi_{ij})$ term (Geist et al., 2009) as described below. This method can be expanded from just examining runup (R) as the hazard variable to producing probabilistic tsunami inundation maps in which wave height and damage metrics are the hazard variables, as discussed in the Seaside, Oregon, Tsunami Pilot Study (Tsunami Pilot Study Working Group, 2006).

A graphic example of how probabilities are aggregated at a particular coastal location is shown in Fig. 1. For this simple case, three source zones are included: two seismogenic zones ($i=1$, $j=1$, 2) generating transoceanic tsunamis and one landslide zone ($i=2$, $j=1$) generating local tsunamis. Zonation for the landslides is primary geographic in this example, based on observed occurrence and distance to the coastal location. More sophisticated zonation schemes can be developed based on geologic factors described by Lee (2009-this issue) and Chaytor et al. (2009-this issue). Zonation for earthquakes in this example is according to plate boundary type (Bird and Kagan, 2004). Source probabilities are given by the rate term ν_{ij} and the size distribution $f(m_j)$ or $f(V_j)$.

If tsunami sources behave in a time-dependent manner (either clustered in time or as a quasiperiodic process), then an aggregation equation other than Eq. (2) needs to be used. The tsunami probability during time T corresponding to each of N sources is calculated and aggregated according to the following equation (Rikitake and Aida, 1988; Ward, 1994):

$$P(R \geq R_0 \,|\, T) = 1 - \prod_{j=1}^{N} \left[1 - P\left(R \geq R_0 \,|\, \psi_j, T\right)\right]. \tag{3}$$

In this case, the set of source parameters ψ_{ij} includes the parameters for the source recurrence distribution.

In the next two sections (3 and 4), we will examine methods to determine the probabilities for both earthquake and landslide tsunami sources, respectively. This includes methods to determine the size distribution f_ψ, overall rate ν_{ij}, and where possible, whether or not earthquakes and landslides are adequately described by a Poisson process in terms of their recurrence distribution.

3. Earthquake tsunamis

In this section, we review different approaches to define the parameters for earthquake size distributions $f(m_j)$. We first focus on

Author's personal copy

earthquake zones in the Caribbean and eastern Atlantic that can potentially generate transoceanic tsunamis and then examine the possibility of seismogenic tsunamis generated locally to the U.S. Atlantic coastline.

3.1. Transoceanic seismogenic tsunamis

For transoceanic tsunamis, seismic moment is the controlling source parameter that determines tsunami amplitude with other parameters having a secondary effect (Okal, 1988; Pelayo and Wiens, 1992; Abe, 1995; Titov et al., 2001). In addition, because only large earthquakes (M_w approximately greater than 8) will result in significant tsunami amplitudes in the far-field, we can focus our attention on earthquakes that occur along plate boundaries, particularly subduction zones and oceanic convergent boundaries (as defined by Bird, 2003). Accordingly, source probabilities can be based on previous statistical work defining seismic moment distributions along plate boundaries (Kagan, 1997; Bird and Kagan, 2004).

3.1.1. Subduction zone boundaries

The Caribbean subduction zone extending from Hispaniola in the west through the Lesser Antilles Islands in the east is the closest plate boundary to the U.S. Atlantic coast along which transoceanic tsunamis can be generated (Fig. 1). Tsunamis generated from large earthquakes along other plate boundary zones in the Caribbean, for example along the northern Venezuela subduction zone and the northern Panama oceanic convergent zone (Bird, 2003) (Fig. 1), are greatly attenuated and scattered as they propagate northward through the Greater Antilles Islands (Knight, 2006), but may result in small tsunami amplitudes at the U.S. Atlantic coast. Most of the historic locally damaging tsunamis recorded along the Greater Antilles segment of the Caribbean subduction zone have been generated by intra-plate events, both along transverse structures such as the Mona rift and back arc structures such as the Muertos and Anegada troughs. Exceptions are the 1946 $M\sim8$ Hispaniola interplate thrust earthquake and subsequent events (Dolan and Wald, 1998; ten Brink and Lin, 2004; Doser et al., 2005). The low rate of subduction earthquakes along this segment can be linked to the highly oblique relative plate motion and slow convergence rates.

The standard Gutenberg–Richter size distribution (G–R) for earthquakes is a power–law magnitude–frequency relationship: $\log N(M_w) = a - bM_w$, where N is the number of earthquakes $\geq M_w$. The tail of the distribution at large sizes is specified in one of two ways:

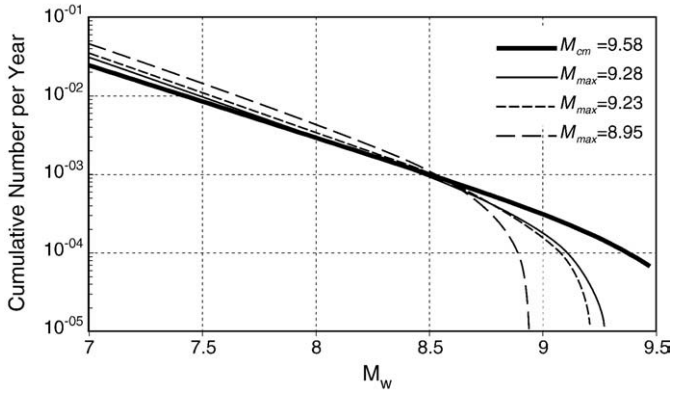

Fig. 2. Comparison of size distributions for earthquakes along the Caribbean subduction zone (Greater Antilles segment). In each case, tectonic moment rates and complete coupling ($\chi = 1$) are used. Truncated G–R distributions computed using three different methods to determine M_{max} and a constant rupture length of 1100 km: moment-length scaling (light solid); moment-area scaling (short dashed); parametric (long dashed). Heavy solid line represents tapered G–R distribution with a maximum-likelihood estimate for M_{cm} from the global earthquake catalog (Bird and Kagan, 2004).

using a sharp truncation specified by a maximum seismic moment M_{max} or using a gradual taper using a corner moment M_{cm} (Kagan, 2002a) as described below. For the former, the size distribution $f(m)$ in Eq. (2) is given by the truncated G–R distribution:

$$f(m) = \beta \frac{(M_{max} m_t)^{\beta}}{M_{max}{}^{\beta} - m_t^{\beta}} m^{-(1+\beta)}, \quad m_t \leq m \leq M_{max}, \tag{4}$$

where m_t is a minimum threshold moment and the power–law exponent $\beta = \frac{2}{3}b$. A similar size distribution with a hard maximum cutoff is specified for tsunamis themselves based on historic data by Burroughs and Tebbens (2005). The maximum moment M_{max} is determined from knowledge of the fault geometry, physical properties, and rupture kinematics such that for a planar fault in an isotropic Earth with no variation in rake

$$M_{max} = \int_{\Sigma} \mu u_s d\Sigma, \tag{5}$$

where μ is the shear modulus and u_s is the static slip for the largest event integrated over the maximum fault area Σ. This is often simplified by using spatial averages of shear modulus ($\overline{\mu}$) and static slip ($\overline{u}_s$) for the largest earthquake such that

$$M_{max} = \overline{\mu}\overline{u}_s\Sigma. \tag{6}$$

Unfortunately, there is significant uncertainty in a parametric approach such as this to determine M_{max}, owing to strong variations in physical properties and kinematics as indicated by past earthquake inversion studies. Often, moment is estimated from scaling relationships with source dimensions (e.g., Mai and Beroza, 2000), rather than using a purely parametric approach. Maximum moment can also be determined from past seismicity as discussed by Kijko (2004). A similar type of distribution is the one in where a large "characteristic" earthquake is identified separately from the background G–R distribution (Wesnousky, 1994). It is unlikely that any of the plate boundary faults in the Atlantic have enough dated paleoseismic horizons to make a statistically meaningful estimate of characteristic magnitude or recurrence (cf., Geist et al., 2009).

A size distribution based on a "soft" corner moment (M_{cm}) is an alternative to the truncated distribution (Eq. (4)) that is more consistent with the available empirical data and with the physics of extreme earthquakes (Sornette and Sornette, 1999; Kagan, 2002a). An example of this type of distribution model that has been fit to global subduction zone seismicity is the tapered G–R distribution (Kagan and Jackson, 2000; Vere-Jones et al., 2001; Kagan, 2002a; Bird and Kagan, 2004):

$$\Phi(m) = \left(\frac{m_t}{m}\right)^{\beta} \exp\left(\frac{m_t - m}{M_{cm}}\right), \quad m_t \leq m, \tag{7}$$

where $\Phi(m)$ is the survivor function ($\Phi(m) = 1 - F(m)$; $F(m)$ is the cumulative distribution of $f(m)$). The two distribution parameters, β and corner moment M_{cm} are estimated by Kagan (1997, 2002a,b) and Bird and Kagan (2004) from the historic earthquake catalog using a maximum log-likelihood method. The difference between the two studies is the way earthquakes are grouped together (i.e., the zonation index j used in this paper): Kagan (2002a,b) analyzes seismicity based on different geographic zonation schemes, whereas Kagan (1997) and Bird and Kagan (2004) group events together based on common plate boundary types. Using the Harvard CMT catalog, the corner moment magnitude $M_{cm} = 8.76 \pm 0.65$ and $\beta = 0.93 \pm 0.43$ for the Lesser Antilles subduction zone (Kagan, 2002b), with the high uncertainty related to the sparse number of events in this region. For global subduction zones using a 20th century earthquake catalog, $M_{cm} = 9.58^{+0.48}_{-0.46}$ and $\beta = 0.64 \pm 0.04$ (Bird and Kagan, 2004).

Unlike the size distribution $f(m_j)$, the rate term υ_{1j} in Eq. (2) that is proportional to the seismic moment rate $\dot{m}_t$ varies substantially

Author's personal copy

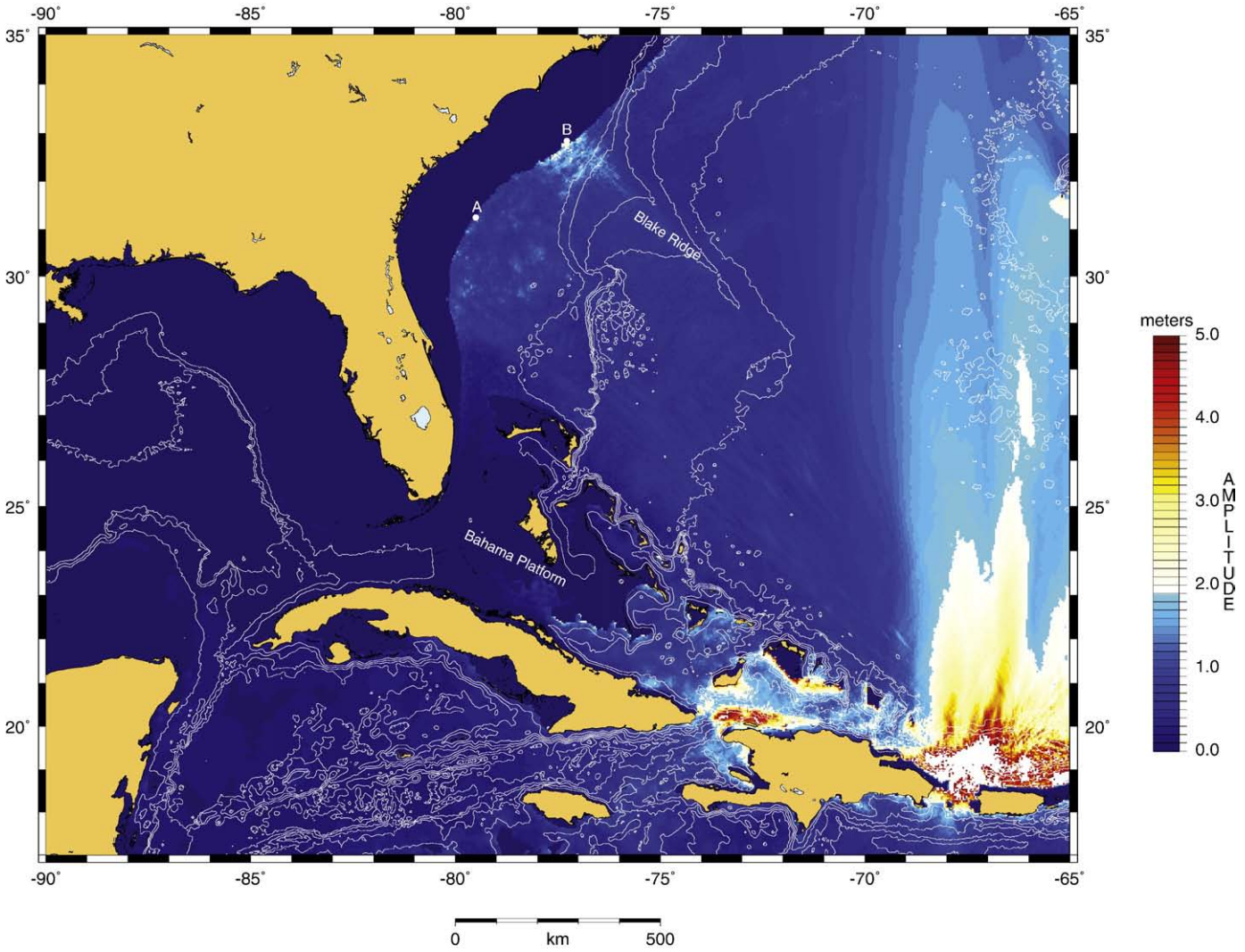

Fig. 3. Example of maximum tsunami amplitude during 4.4 h of total propagation time for a $M \sim 9$ earthquake on the Caribbean subduction zone. Tsunami beaming is apparent along an azimuth perpendicular to strike, although the Blake Ridge acts as a waveguide to locally focus tsunami energy. Points A and B discussed in Fig. 4 shown for reference.

among subduction zones, depending principally on relative plate convergence rate and seismic coupling (McCaffrey, 1994; Kagan, 2002b; Kreemer et al., 2002; Bird and Kagan, 2004). The rate term can be related to the seismic moment rate ($\dot{m}_{s(j)}$) for size distributions indicated in Eqs. (4) and (7), respectively, as described by Kagan (2002b) (cf., McCaffrey, 1994):

$$\upsilon_j(m) = \frac{(1-\beta)\dot{m}_{s(j)}\left(M_{\max}^{\beta} - m^{\beta}\right)}{\beta m^{\beta} M_{\max}} \tag{8}$$

and

$$\upsilon_j(m) = \frac{(1-\beta)\dot{m}_{s(j)}}{m^{\beta} M_{\mathrm{cm}}^{1-\beta}\Gamma(2-\beta)e^{m/M_{\mathrm{cm}}}}, \tag{9}$$

where Γ is the gamma function. The "tectonic" moment rate ($\dot{m}_{t(j)}$) is given by

$$\dot{m}_{t(j)} = \mu_j L_j W_j \dot{s}_j, \tag{10}$$

where μ is the shear modulus, L is the length of the fault zone, W is the width of the seismogenic part of the fault zone, and $\dot{s}$ is the long-term slip rate along the fault determined from geodetic and plate motion studies (McCaffrey, 1994; Ward, 1994). It should be noted that there is a strong depth dependence in μ for subduction zones (Bilek and Lay, 1999), such that the value used in Eq. (10) is an average over the entire zone. $\dot{m}_s$ and $\dot{m}_t$ are related by a seismic coupling parameter ($0 \le \chi \le 1$): $\dot{m}_s = \chi \dot{m}_t$. For a fault that has no aseismic slip at seismogenic depths, $\chi = 1$. For the Caribbean subduction zone, $\dot{m}_s$ is more than an order of magnitude less than $\dot{m}_t$ (4.0×10^{18} Nm/yr compared to 4.9×10^{19} Nm/yr) (Kagan, 2002b), suggesting that either χ is very low or that the historic catalog is under-sampled, particularly with respect to large magnitude earthquakes that dominate estimates of $\dot{m}_s$ (cf., Parsons and Geist, in press). Compounding this discrepancy, Caribbean subduction zone slip rates may be considerably higher than the NUVEL-1A (DeMets et al., 1994) plate-rate model used by Kagan (2002b). For example, Dixon et al. (1998) and DeMets et al. (2000) calculated a Caribbean plate rate of 21 ± 1 mm/yr and 18–20 ± 3 mm/yr, respectively, from GPS measurements, nearly twice the NUVEL-1A estimate of 11 ± 3 mm/yr.

A comparison of several different frequency–magnitude distributions for the Caribbean subduction zone using the tectonic moment rate derived from regional slip rates and a seismic coupling parameter $\chi = 1$ is shown in Fig. 2. For the truncated G–R distribution (Eq. (4)), a maximum 1100 km fault length was assumed (from Hispaniola to the Caribbean–N. America–S. America triple junction) and three different methods were considered to determine $M_{\max}$. The light solid line

Author's personal copy

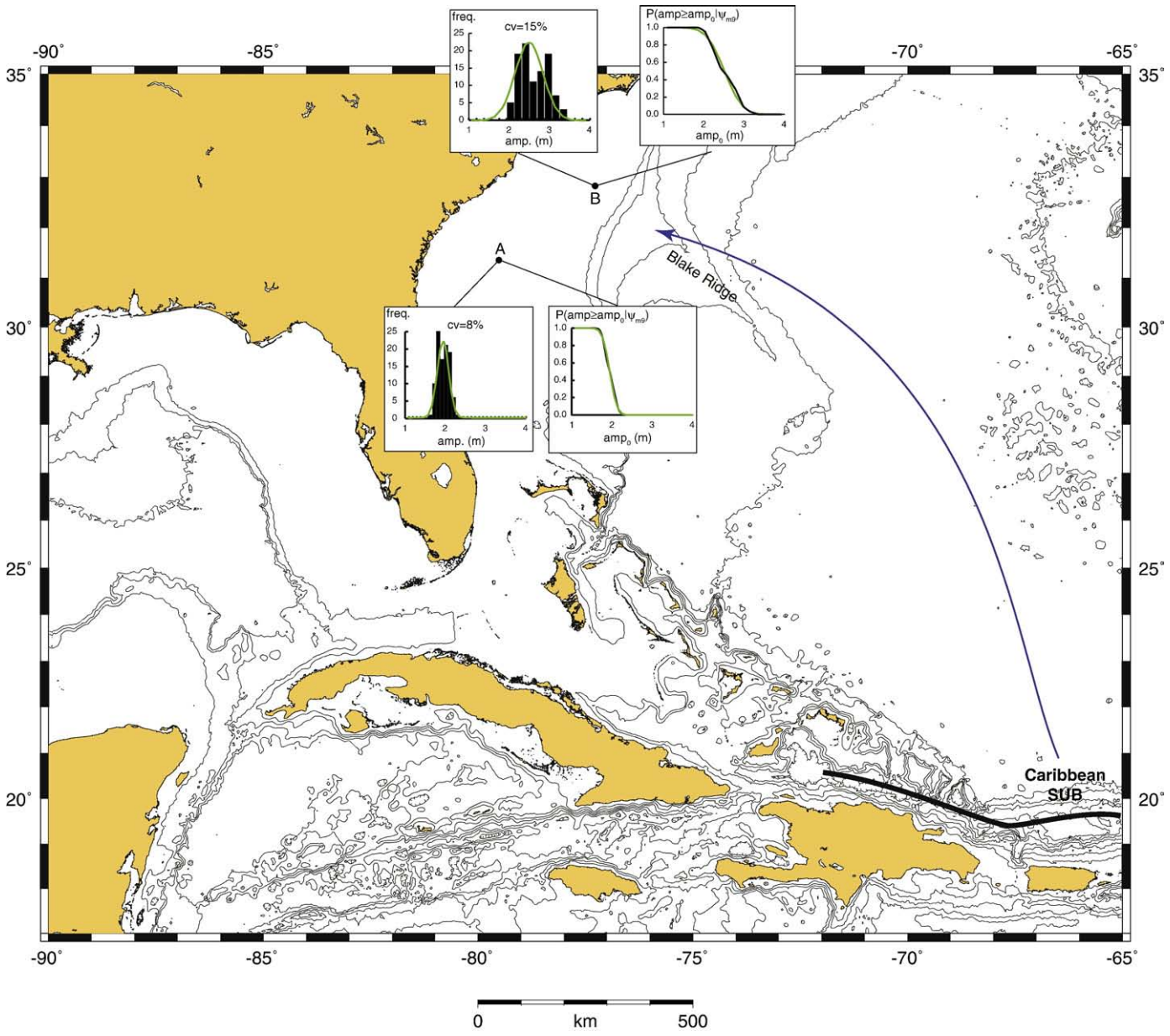

Fig. 4. Examples of the probability that tsunami amplitude will exceeded a given value $P(\text{amp} \geq \text{amp}_0|\psi_{M\,9})$, for 2 different sites (A and B) along the Atlantic coast and the same $M \sim 9$ earthquake along the Caribbean subduction zone. Left plot: Histogram of amplitude values as a results of varying slip distribution patterns for the source earthquake (cv—coefficient of variation). Green line represents normal distribution approximation. Right: Probability of exceeding amplitude value amp_0 using the histogram values (black line) and the normal distribution approximation (green line).

represents moment-length scaling (Mai and Beroza, 2000), the short-dashed line moment-area scaling (Wyss, 1979), and the long-dashed line a parametric approach with $\overline{\mu} = 30$ GPa and $\overline{u}_s = 9$ m (Eq. (6)). The heavy solid line represents the tapered G–R distribution (Eq. (7)) with the maximum-likelihood estimate for M_{cm} from the Bird and Kagan (2004) study (it should be noted that this study also provides 95% confidence interval estimates for M_{cm}). For a higher M_{max} or M_{cm}, the overall activity (a-value) has to decrease to balance the overall moment rate.

For a given source size, the probability that runup will exceed R_0 at a coastal location for source parameters ψ_{ij} is given by the term $P(R > R_0|\psi_{ij})$ in Eq. (2). Shown in Fig. 3, for example, is the maximum tsunami wavefield from a $M_{\text{w}} \sim 9$ earthquake along the Caribbean subduction zone computed using a finite-difference approximation to the linear long-wave propagation equations. Details of the tsunami generation and propagation methods used to construct Fig. 3 are described in Geist (2002) and Geist et al. (2007). To determine the uncertainty from different slip distribution patterns $u(x,y)$ during earthquake rupture on tsunami amplitude, $P_{M=9}(\text{amp} > \text{amp}_0|\, u(x,y))$ was calculated for two points offshore the U.S. Atlantic coast spaced 230 km apart, where maximum offshore amplitude (amp) is used as the hazard variable rather than runup (R) (Fig. 4). The histograms for each site show the maximum amplitude from 100 different slip distributions. Uncertainty caused by this source parameter can be approximated by a normal distribution (green line), though in some cases (e.g., Point B in Fig. 4) the distribution of wave amplitudes is multi-modal. The exceedance probability $P_{M=9}(\text{amp} > \text{amp}_0|\, u(x,y))$ varies significantly between the two points shown, owing to wave propagation—particularly the waveguide effect of the Blake Ridge (Fig. 1). Multiple sources of uncertainties in evaluating $P(R > R_0|\psi_{ij})$ can be accommodated using Monte Carlo techniques (Geist and Parsons, 2006).

Author's personal copy

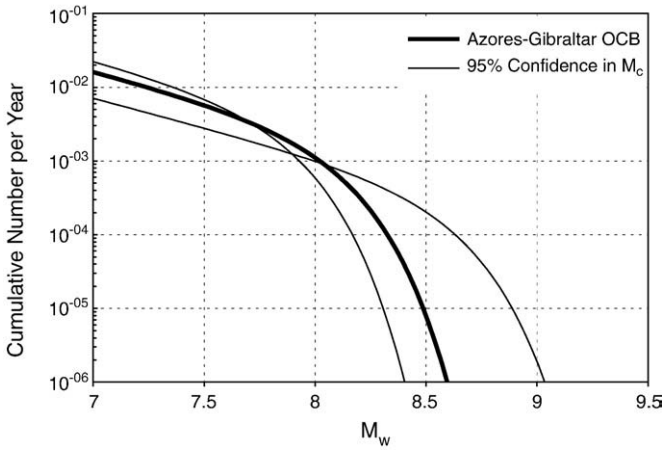

Fig. 5. Comparison of size distributions for earthquakes along the Azores–Gibraltar oceanic convergence boundary. Size distributions were computed using tectonic moment rates and distribution shape parameters from Bird and Kagan (2004). Heavy line represents tapered G–R distribution with a maximum-likelihood estimate for M_c from the global earthquake catalog; thin lines represent distributions for 95% confidence interval in M_c (Bird and Kagan, 2004).

Finally, the recurrence distribution for subduction zone earthquakes most closely follows an exponential distribution (Eq. (1)), with some exceptions. Several studies (Kagan and Jackson, 1991, 1995; Rong et al., 2003) test the seismic gap hypothesis based on time-dependent recurrence against a Poisson null hypothesis related to the exponential distribution of recurrence times and found that in most cases the Poisson null hypothesis passed most of the statistical tests. Clustering of earthquakes in time as characterized by greater number of short inter-event times than expected from an exponential distribution is evident in most global earthquake catalogs. This is usually attributed to aftershocks and other triggered earthquakes (Parsons, 2002) and has been explained using a negative binomial distribution (Kagan and Jackson, 2000) or a gamma distribution (Corral, 2004).

3.1.2. Non-subduction zone boundaries

Other non-subduction zone boundaries in the Atlantic where tsunamigenic earthquakes can occur include the Azores–Gibraltar oceanic convergence boundary (Fig. 1). It was here that the 1755 and 1761 Lisbon earthquakes generated transoceanic tsunamis recorded in the Lesser Antilles Islands (O'Loughlin and Lander, 2003; Baptista, 2006). This boundary is structurally complex with convergence in the eastern part indicated from deformation modeling (Jiménez-Munt et al., 2001) and the mechanism of the $M_w = 7.8$, 1969 Cape St. Vincent (Portugal) earthquake (Fukao, 1973). Sources for the tsunamis in this zone include the Gorringe Bank faults and the shallow, eastward dipping thrust faults in the Horseshoe abyssal plain and the Gulf of Cadiz (Gjevik et al., 1997; Baptista et al., 2003; Gràcia et al., 2003; Terrinha et al., 2003; Zitellini et al., 2004; Gutscher et al., 2006; Thiebot and Gutscher, 2006). The geometry of the fault zone and its position relative to mid-ocean topographic features that scatter tsunami energy have important controls on tsunami amplitudes along the U.S. Atlantic coast (Barkan et al., 2008-this issue). Although there is insufficient seismic activity along this zone to determine the seismic moment distribution, for oceanic convergent zones on a global basis, $M_{cm} = 8.04^{+0.52}_{-0.22}$ and $\beta = 0.53 \pm 0.13$ (Bird and Kagan, 2004). Determination of M_{ma} for the truncated G–R size distribution would entail determining the interaction of the different fault strands that make up this plate boundary (cf., Ward, 1997).

Gutscher et al. (2006) indicate that for a 1 cm/yr convergence rate, an event similar to the M_w 8.6–8.8 1755 earthquake would occur with a mean return time of 1000–2000 years. This estimate may be on the low side, as recent GPS surveys indicate lower convergence rates, ranging from 1 to 5 mm/yr (Fernandes et al., 2003; Nocquet and Calais, 2004). Using the lower convergence rate and a tapered G–R distribution results in a much higher mean return time for an event like the 1755 earthquake (Fig. 5), though there is significant uncertainty in magnitude distributions for OCB boundaries. This demonstrates the critical effect that corner moment and plate-rate estimates have on estimating seismogenic tsunami source probabilities.

Mid-ocean spreading ridges, such as the mid-Atlantic ridge, are unlikely to generate transoceanic tsunamis because of a low corner magnitude $M_{cm} = 5.82 \pm 0.07$ (Bird et al., 2002). Oceanic transform faults have a higher corner magnitude, but because there is little vertical displacement associated with strike-slip earthquakes, tsunamis emanating from theses fault zones are typically very small.

3.2. Local tsunamigenic earthquakes

In addition to earthquakes generating transoceanic tsunamis, it is possible that offshore earthquakes within the North American plate may generate local tsunamis. Seismicity is broadly distributed along the U.S. Atlantic coast and not concentrated on identified fault zones (Kafka and Levin, 2000; Kafka, 2002). Compared with active tectonic margins, which are often dominated seismically by one-to-several faults, earthquake magnitudes and rates of seismicity are significantly smaller along the passive margin of the eastern U.S. In this region, recent seismicity is relatively greater along the northern Atlantic seaboard than the southern (with the exception of the 1886 Charleston earthquake and aftershocks), as are strain rates determined from seismic and GPS observations (Anderson, 1986; Gan and Prescott, 2001). This in turn can be linked to isostatic rebound following glaciation in the north as well as overall differences in the crustal structure between the two regions (Wheeler, 1996). Kafka and Levin (2000) suggest that the broad seismicity patterns defined by small earthquakes tend to delineate where large earthquakes may occur. In addition, Ebel and Kafka (2002) indicate that earthquakes are more clustered in time than predicted by a Poisson process.

The size distribution for this region based on past seismicity patterns (Frankel, 1995; Frankel et al., 1996; Wheeler and Frankel, 2000; Frankel et al., 2002) has been described using a truncated Gutenberg–Richter distribution where the moment rate and power–law exponent (β) are determined from gridded and smoothed seismicity. In these studies, the G–R distribution is truncated (in the cumulative form of the distribution) at $M_w = 7.5$. As an alternative, one may choose a smooth taper using the distributions described, for example, by Kagan (2002a). Like transoceanic tsunamis, estimating the tail of the distribution becomes a critical issue for calculating local tsunami probabilities, since only earthquakes of $M_w > 6.5$–7.0 generate significant local tsunami amplitudes (Geist, 1999).

The studies indicated above were designed for assessing onshore seismic hazard and were not intended to extend offshore (Frankel et al., 1996). A persistent problem in determining the rates of seismicity in the offshore region (υ_{1j}) is catalog completeness. Mazzotti and Adams (2005) address this problem offshore eastern Canada by comparing different zonation schemes based either on patterns of historic seismicity or on geologic and tectonic boundaries. For the latter model, they indicate relatively high seismic moment rates along the eastern continental margin where the 1929 Grand Banks earthquake occurred. Analysis of seismicity can be combined with geodetic studies (e.g., Gan and Prescott, 2001) to help reduce the uncertainty in estimating the rate of earthquake activity. ten Brink et al. (2009-this issue) estimates a wide range of return times (600–3000 years) for $M_w > 7.0$ earthquakes using the available data and analyses. In terms of seismic moment rates, the maximum rate in the coastal region estimated by Gan and Prescott (2001) is approximately 6×10^{16} Nm/yr, i.e. several orders of magnitude less that the ~10^{20} Nm/yr rate for the Caribbean subduction zone.

Author's personal copy

Although earthquake magnitude is the primary source parameter, other parameters such as average slip, fault mechanism, and focal depth also significantly affect local tsunami amplitudes (Geist, 1999). Stress drops associated with intra-plate earthquakes, particularly in the eastern U.S., are variable but do not indicate a distinct scaling relationship with seismic moment relative to western U.S. earthquakes (Somerville et al., 1987; Hartzell et al., 1994). Most focal solutions for eastern North American earthquakes indicate a predominantly near horizontal axis of compression with a mixture of reverse, strike slip, or composite mechanisms (Hartzell et al., 1994; Bent, 1995; Du et al., 2003; Mazzotti and Adams, 2005). Focal depths are typically shallow for U.S. events (2–8 km) and slightly deeper for Canadian events (5–28 km) (Du et al., 2003).

4. Landslide tsunamis

Like submarine earthquakes, only large landslides can potentially generated significant tsunamis. Although we focus on submarine landslides here, it should be recognized that subaerial landslides can generate impact tsunami with dramatic runup in the near field (Fritz et al., 2001; Fritz, 2006). In contrast to submarine earthquakes, submarine landslide probabilities are more difficult to determine because a lack of an instrumental catalog of occurrence. From the NGDC global tsunami catalog, less than 10% of all tsunamis are estimated to have a landslide-generation component, though observations of landslide sources are likely to be incomplete. Recent marine geophysical surveys have helped define the volume distribution of landslides in specific regions (Booth et al., 1993; Chaytor et al., 2009-this issue), but the lack of a complete catalog of age dates for individual landslides precludes accurate assessment of the recurrence distribution and overall activity rate υ_{2j}. One advantage over earthquake tsunami sources is that landslide probabilities typically only have to be determined for sources local to the coastal location, rather than throughout an entire ocean basin. Although the largest landslides may generate transoceanic tsunamis of significant amplitude, recent studies (e.g., Gisler et al., 2006 for the Canary Islands landslide tsunami) indicate that non-linear and dispersive effects greatly attenuate tsunami energy at far-field distances in comparison to seismogenic tsunamis.

4.1. Empirical methods

Empirical methods to determine the source rate term υ_{2j} or the recurrence distribution of offshore landslides have primarily been hampered by a lack of age dates. As an initial hypothesis, we can assume that the recurrence distribution is that of a Poisson process, although an initial study of onshore landslides in Italy (Rossi et al., 2007) suggests that landslides are more clustered in time than predicted by an exponential distribution (1). Clustering of terrestrial landslides may result in part from climatic conditions and/or seismic triggers (e.g., Kang and Wang, 1995; Chleborad, 1997; Trauth et al., 2003): processes that may influence temporal distributions of submarine landslides as well. As such, nearshore processes might depart from a Poisson process at short inter-event times. Given a minimum number of landslide ages, we may be able to adapt recently developed methods to establish source probabilities from observed, uncertain event times for earthquakes (Ogata, 1999; Parsons, 2008) to landslide probabilities if the form of the inter-event distribution can be assumed and some temporal record exists.

It should be noted that results described by Maslin et al. (2004) and Lee (2009-this issue) suggests that the long-term recurrence rate of landslides may be dependent on glacial cycles. For the U.S. and Canadian Atlantic margin, Lee (2009-this issue) indicates dates for two of the largest landslides: the Cape Fear landslide (9–14.5 kyr) and the Currituck landslide (25–50 kyr) (Fig. 1). From the available age dates, relatively few landslides occur in more recent times (i.e., >5000 years after the end of glaciation). The tsunamigenic 1929 Grand Banks landslide (Piper et al., 1999) is a notable exception. Lee (2009-this issue) estimates that the rate of landslide occurrence during the last 5000 years is 2.5–3.5 times less than during the last glacial, deglaciation period. Therefore, over 10's of thousands of years the distribution of landslide occurrence times is likely that of a non-stationary Poisson process such that the rate term υ_{2j}, decreases with time since the last glacial period. Adapting either Ogata's (1999) Bayesian inference approach or Parsons' (2008) Monte Carlo approach to landslide probabilities would require, therefore, that the inter-event distribution class for which parameter estimation is conducted be non-stationary.

Statistical studies of onshore landslides have indicated that the size distribution is essentially a power law over a large range of volumes ($f(V_j)$ in Eq. (2) above). Taking into account very small and very large volumes, more complex size distributions that span the observed range of volumes are described by a number of authors (Stark and Hovius, 2001; Guzzetti et al., 2002; Dussauge et al., 2003; Malamud et al., 2004; Chaytor et al., 2009-this issue).The origin of power–law scaling appears to require a state variable that results in a long-term, time-weakening effect (Hergarten and Neugebauer, 1998; Hergarten, 2003), arising from, for example, strain softening, creep, and pore-pressure redistribution. In addition, it appears that the power–law exponent of the distribution is dependent on the type of failure (e.g., rock fall, slump, etc.) and the lithology of the failed material (Dussauge et al., 2003; Malamud et al., 2004). In the offshore region, examination of landslides north of Puerto Rico have established that landslide volumes (V) also follow a power–law relationship, with an exponent similar to that observed for onshore rock falls (ten Brink et al., 2006).

4.2. Link to earthquake ground motions

Because the majority of (but not all) tsunamigenic landslides are triggered by earthquakes (Bardet et al., 2003), landslide probabilities can also be inferred from earthquake ground motions and a slope stability model as an alternative to a direct empirical approach. From an earthquake scenario-based mode, Jibson et al. (2000) shows that if the topography, geology, shear strength and seismic shaking for a given earthquake are known, then one can determine the probability of failure over a certain region. Shear strength is likely one of the greatest unknowns, particularly in the marine environment where direct tests over a given region may be limited. More generally, landslide probabilities can be linked to probabilistic ground motions based on a distribution of earthquake magnitudes. We can think of the probability that a landslide of a certain size will occur (P_V) in terms of the probability of the triggering event E (i.e., seismic ground motion above a certain level: $P(E)$) and the conditional, time-dependent probability of threshold or preparatory conditions leading to an outcome O of slope failure (cf., Lee et al., 2001):

$$P_V = P(E)P(O|E,t). \tag{11}$$

Threshold conditions would include slope angle, shear strength, groundwater flow conditions, sediment load, gas hydrate dissociation, etc. (Locat and Lee, 2002; Biscontin et al., 2004; Maslin et al., 2004; Biscontin and Pestana, 2006; Lee, 2008-this issue). $P(E)$ can be determined straightforwardly from PSHA, using an appropriate spectral acceleration relative to the thickness of the near surface layer that can fail (Biscontin et al., 2004; Biscontin and Pestana, 2006). The probability $P(O|E)$, however, would have to be computed using a complex event tree in which the uncertainties are likely to be large. For example Wright and Rathje (2003) and Biscontin et al. (2004) indicate that the nature of pore-pressure redistribution following an earthquake that can cause delayed initiation of a failure is related to the physical properties of the near surface layer. Hence, the preparatory conditions for landslide failure are likely to be time dependent as indicated in Eq. (11).

Author's personal copy

This problem can be simplified by using empirical relationships between earthquake magnitude and ensemble landslide statistics such as total area or volume, maximum distance to failure, etc. (Keefer, 1994, 2002). ten Brink et al. (2009-this issue) adapts this type of approach to determine the minimum magnitude and maximum distance from the continental shelf edge for earthquakes to trigger landslides of tsunamigenic size. That study indicates that the width of a potential landslide hazard zone is dependent on the magnitude of the earthquake. The rate at which landslides above a certain volume occur along the continental slope can then be tied to the rate of earthquake occurrence within the zone where triggering may occur. Although there are large uncertainties with this approach, it is a useful way to estimate the rate of landslide occurrence until more age dates become available.

5. Discussion

5.1. Comparative analysis of different tsunami sources

Assessment of source probabilities for tsunamis affecting the U.S Atlantic coast yield comparative information with which to better define the scope of the hazard. For example, the mean return time for $M_w > 8.0$ earthquakes that potentially can generate transoceanic tsunamis along the Caribbean subduction zone (Fig. 2) is greater than that along Azores–Gibraltar convergence zone (Fig. 5). If we use source rates for each of these zones of $\sim 2.5 \times 10^{-3}$ yr^{-1} and $\sim 1.0 \times 10^{-3}$ yr^{-1} respectively, then the mean return time of a tsunami exceeding $R_0(M_w > 8.0)$ (where, R_0 is the minimum runup from either of the two source zones) is ~285 years. For $M_w > 8.5$ earthquakes along these two source zones, and considering the significant uncertainty in the size distribution for the Azores–Gibraltar convergence zone, the mean return time of a tsunami exceeding $R_0(M_w > 8.5)$ is 800–1000 years. Because runup scales directly with seismic moment, $R_0(M_w > 8.5)$ will typically be greater than $R_0(M_w > 8.0)$.

In comparison to the previous example, the few available age dates of large landslides that might generate tsunamis local to the northern U.S. Atlantic coast suggest that the mean rate is $\sim 10^{-4}$ yr^{-1}, with higher rates along the Canadian Atlantic coast (Lee, 2009-this issue). As indicated by Lee (2009-this issue), the mean rate may be decreasing with time since the last glacial period. It should be stressed, however, that there are currently few age dates for landslides along the Atlantic margin, such that the observed rate may be biased (under-sampled). Even so, there is likely little contribution from landslide tsunamis according to the aggregation in Eq. (2), if one were concerned about tsunamis occurring at, for example, an annual probability of $P = 0.005$ (i.e., a 200-year return time tsunami). This is consistent with the overall low incidence of landslides tsunamis from the global historic catalog. The mean return time for local seismogenic sources ($M_w > 7$) in the northern U.S. Atlantic coast is 600–3000 years (ten Brink et al., 2009-this issue) and thus may span the mean recurrence rates of transoceanic sources and local landslide sources.

5.2. Uncertainties

For an accurate tsunami probabilistic assessment, however, there is still significant uncertainty in these source probabilities. Probabilistic methods accommodate model and parameter uncertainty by classifying them as either epistemic (uncertainty that will decrease with the acquisition of additional data) or aleatory (natural or stochastic uncertainty) (Toro et al., 1997). Examples of epistemic uncertainty alluded to in this study include different methods to determine M_{max} (Fig. 2), different estimates of the seismic coupling parameter χ, and different estimates of fault slip rates. Epistemic uncertainty is typically accommodated in PTHA through the use of logic trees (e.g., Geist and Parsons, 2006) or a Bayesian weighting scheme (Parsons and Geist, in press). Examples of aleatory uncertainty include slip distribution (Fig. 4) and tidal stage at the time of tsunami arrival (Mofjeld et al., 2007). Aleatory uncertainty is typically accommodated by integration in the $P(R > R_0|\psi_{ij})$ term in Eq. (2) (Geist et al., 2009). Special considerations need to be taken in probabilistic methods when different sources of uncertainty are dependent on one another (Page and Carlson, 2006).

For tsunamis affecting the U.S. Atlantic coast, the greatest uncertainty is associated with landslide probabilities. Not only is there little information on the shape of the recurrence distribution, but even information on the overall mean rate of occurrence is lacking because of few available age dates. There are statistical methods to estimate recurrence rates from sparse and uncertain data (Ogata, 1999; Parsons, 2008). These techniques have been designed for estimating earthquake recurrence rates using paleoseismic horizons associated with a range of age dates. Similarly, these techniques can be applied to landslides, once a range of age dates is obtained from strata above and below a landslide geologic unit (Lee, 2005).

5.3. Future directions

In contrast to determining landslide recurrence rates, determining the size distribution for landslides is currently a tractable problem. Modern marine geophysical methods and GIS tools permit a fairly accurate determination of landslide volumes over broad reaches of seafloor (Chaytor, 2009-this issue). Moreover, recent advances in modeling the dynamics and mobility of submarine landslides (Imran et al., 2001; Locat et al., 2004; Locat et al., 2009-this issue) permit a reasonable determination of landslide motion—a significant parameter affecting tsunami generation (Harbitz, 1992; Ward, 2001; Grilli and Watts, 2005; Løvholt et al., 2005; Brandshaw et al., 2007). Development of tsunami models that explicitly solve for landslide and wave dynamics as part of a coupled system will provide even more accurate estimates of wave heights and runup.

For earthquakes, although the earthquake catalog for the Caribbean subduction zone and the Azores–Gibraltar oceanic convergence zone is sparse and incomplete, seismic moment rate can be inferred from tectonic motions and geodetically determined fault slip rates. In addition, the parameters for the size distribution can be estimated using global earthquakes specific to different plate boundaries as performed by Kagan (1997) and Bird and Kagan (2004). However, generation of transoceanic tsunamis occurs for earthquakes of large magnitude ($M_w \geq 8$) and is therefore sensitive to the shape of the size distribution tail and corner moment magnitude M_{cm} as indicated in Figs. 2 and 5. Further work is needed to better constrain these parameters, especially for oceanic convergent boundaries. In terms of the recurrence distribution, whereas the exponential distribution associated with a Poisson process is a good first approximation, there appear to be cases of time-dependency which may also affect tsunami probability calculations.

6. Conclusions

Because of the sparse record of tsunamis along the U.S. Atlantic coast, tsunami probability needs to be determined from a computational PTHA approach, rather than using only empirical methods based on tsunami catalogs. Key ingredients in the computational approach are the probability distribution of tsunami source sizes and source recurrence. For the most frequent source of tsunamis, earthquakes along subduction and oceanic convergent plate boundaries in the Atlantic, the shape of these distributions can be inferred from studies of global seismicity (e.g., Bird and Kagan, 2004). For other less frequent sources of local tsunamis, including offshore intra-plate earthquakes and landslides, it is more difficult to determine the size and inter-event distribution because of a lack of recorded events and the geographically distributed nature of these events. For landslides, the size distributions and overall rate of occurrence can be determined from the available sparse age dates in combination with global comparison of potentially tsunamigenic landslides (e.g., Lee, 2009-this issue), and through an association with triggering earthquakes (e.g., ten Brink et al., 2009-this issue).

Author's personal copy

The highest rate of earthquake activity that could produce transoceanic tsunamis in the Atlantic occurs along Caribbean subduction zone and Azores–Gibraltar oceanic convergence zones. For $M_w \geq 8.0$ earthquakes, for example, rates along the Caribbean subduction zone are approximately 2.5 times that for the Azores–Gibraltar oceanic convergence zone, with an aggregate return time of ~285 years for transoceanic tsunamis. For $M_w \geq 8.5$ earthquakes, the rate along the Caribbean subduction zone is at least 5 times greater than that for the Azores–Gibraltar oceanic convergence zone, resulting in an aggregate return time of ~800–1000 years. Local landslide tsunamis, may occur at rates approximately an order of magnitude less than for transoceanic tsunamis, although there are few age dates of submarine landslides to validate this estimate. In terms of the recurrence distribution, deviations from the standard Poisson assumption for source inter-event times include clustering for earthquake sources and non-stationarity for landslide sources. There is currently a high level of uncertainty associated with tsunami probabilities in the Atlantic that can be improved with the acquisition of additional marine geologic and geophysical data and further statistical analyses.

Acknowledgements

This paper greatly benefited from constructive comments provided by Mark Petersen, Homa Lee, the managing guest editor, and three anonymous reviewers.

References

Abe, K., 1995. Estimate of tsunami run-up heights from earthquake magnitudes. In: Tsuchiya, Y., Shuto, N. (Eds.), Tsunami: Progress in Prediction, Disaster Prevention and Warning. Kluwer Academic Publishers, Dordrecht, pp. 21–35.
Anderson, J.G., 1986. Seismic strain rates in the central and eastern United States. Bull. Seismol. Soc. Am. 76, 273–290.
Baptista, M.A., 2006. In search of the 31 March 1761 earthquake and tsunami source. Bull. Seismol. Soc. Am. 96, 713–721.
Baptista, M.A., Miranda, J.M., Chierici, F., Zitellini, N., 2003. New study of the 1755 earthquake source based on multi-channel seismic survey data and tsunami modeling. Nat. Hazards Earth Syst. Sci. 3, 333–340.
Bardet, J.-P., Synolakis, C.E., Davies, H.L., Imamura, F., Okal, E.A., 2003. Landslide tsunamis: recent findings and research directions. Pure Appl. Geophys. 160, 1793–1809.
Barkan, R., ten Brink, U.S., Lin, J., 2008. Far field tsunami simulations of the 1755 Lisbon earthquake: Implications for tsunami hazard to the U.S. East Coast and the Caribbean. Mar. Geol. 264, 109–122 (this issue).
Bent, A.L., 1995. A complex double-couple source mechanism for the Ms 7.2 1929 Grand Banks earthquake. Bull. Seismol. Soc. Am. 85, 1003–1020.
Bilek, S.L., Lay, T., 1999. Rigidity variations with depth along interplate megathrust faults in subduction zones. Nature 400, 443–446.
Bird, P., 2003. An updated digital model of plate boundaries. Geochem., Geophys., Geosyst. 4. doi:10.1029/2001GC000252.
Bird, P., Kagan, Y.Y., 2004. Plate-tectonic analysis of shallow seismicity: apparent boundary width, beta-value, corner magnitude, coupled lithosphere thickness, and coupling in 7 tectonic settings. Bull. Seismol. Soc. Am. 94, 2380–2399.
Bird, P., Kagan, Y.Y., Jackson, D.D., 2002. Plate tectonics and earthquake potential of spreading ridges and oceanic transform faults. In: Stein, S., Freymueller, J.T. (Eds.), Plate Boundary Zones. American Geophysical Union, Geodynamic Series, Washington, D.C., pp. 203–218.
Biscontin, G., Pestana, J.M., 2006. Factors affecting seismic response of submarine slopes. Nat. Hazards Earth Syst. Sci. 6, 97–107.
Biscontin, G., Pestana, J.M., Nadim, F., 2004. Seismic triggering of submarine slides in soft cohesive soil deposits. Mar. Geol. 203, 341–354.
Booth, J.S., O'Leary, D.W., Popenoe, P., Danforth, W.W., 1993. U.S. Atlantic continental slope landslides: their distribution, general attributes, and implications. In: Schwab, W.C., Lee, H.J., Twichell, D.C. (Eds.), Submarine Landslides: Selected Studies in the U.S. Exclusive Economic Zone. U.S. Geological Survey Bulletin, vol. 2002, pp. 14–22.
Brandshaw, A.S., Baxter, C.D.P., Taylor, O.-D.S., Grilli, S.T., 2007. Role of soil behavior on the initial kinematics of tsunamigenic slides. In: Lykousis, V., Sakellariou, D., Locat, J. (Eds.), Submarine Mass Movements and Their Consequences. Springer, pp. 387–394.
Burroughs, S.M., Tebbens, S.F., 2005. Power law scaling and probabilistic forecasting of tsunami runup heights. Pure Appl. Geophys. 162, 331–342.
Chaytor, J.D., ten Brink, U.S., Solow, A.R., Andrews, B.D., 2009. Size distribution of submarine landslides along the U.S. Atlantic Margin and its implication to tsunami hazards. Mar. Geol. 264, 16–27 (this issue).
Chleborad, A.F., 1997. Temperature, snowmelt, and the onset of spring season landslides in the central Rocky Mountains. Open-File Report 97-27, U.S. Geological Survey, 18 pp.
Corral, A., 2004. Long-term clustering, scaling, and universality in the temporal occurrence of earthquakes. Phys. Rev. Lett. 92. doi:10.1103/PhysRevLett.92.108501.
DeMets, C., Gordon, R.G., Argus, D.F., Stein, S., 1994. Effect of recent revisions to the geomagnetic reversal time scale on estimates of current plate motions. Geophys. Res. Lett. 21, 2191–2194.
DeMets, C., et al., 2000. GPS geodetic constraints on Caribbean–North America plate motion. Geophys. Res. Lett. 27, 437–440.
Dixon, T.H., et al., 1998. Relative motion between the Caribbean and North American plates and related boundary zone deformation from a decade of GPS observations. J. Geophys. Res. 103, 15,157–15,182.
Dolan, J.F., Wald, D.J., 1998. The 1943–1953 north-central Caribbean earthquakes: active tectonic setting, seismic hazards, and implications for Caribbean–North America plate motion s. In: Dolan, J.F., Mann, P. (Eds.), Active Strike-Slip and Collisional Tectonics of the Northern Caribbean Plate Boundary Zone. Geological Society of America, Special Paper, vol. 326, pp. 143–169. Boulder, Colorado.
Doser, D.I., Rodriguez, C.M., Flores, C., 2005. Historical earthquakes of the Puerto Rico–Virgin Islands region (1915–1963). In: Mann, P. (Ed.), Active Tectonics and Seismic Hazards of Puerto Rico, the Virgin Islands, and Offshore Areas. Geological Society of America, Special Paper, vol. 385, pp. 103–114. Boulder, Colorado.
Du, W.-X., Kim, W.-Y., Sykes, L.R., 2003. Earthquake source parameters and state of stress for the northeastern United States and southeastern Canada from analysis of regional seismograms. Bull. Seismol. Soc. Am. 93, 1633–1648.
Dussauge, C., Grasso, J.R., Helmstetter, A., 2003. Statistical analysis of rockfall volume distributions: implications for rockfall dynamics. J. Geophys. Res. 108. doi:10.1029/2001JB000650.
Ebel, J.E., Kafka, A.L., 2002. A non-Poissonian element in the seismicity of the northeastern United States. Bull. Seismol. Soc. Am. 92, 2040–2046.
Fernandes, R.M.S., Ambrosius, B.A.C., Noomen, R., 2003. The relative motion between Africa and Eurasia as derived from the ITRF2000 and GPS data. Geophys. Res. Lett. 30. doi:10.1029/2003GL017089.
Frankel, A.D., 1995. Mapping seismic hazard in the central and eastern United States. Seismol. Res. Lett. 66, 8–21.
Frankel, A.D. et al., 1996. National seismic-hazard maps: Documentation June 1996. 96–532, U.S. Geological Survey, 41 pp.
Frankel, A.D. et al., 2002. Documentation for the 2002 Update of the National Seismic Hazard Maps. 02-420, U.S. Geological Survey, 33 pp.
Fritz, H.M., 2006. Physical modeling of landslide generated tsunami. In: Mercado, A., Liu, P.L.F. (Eds.), Caribbean Tsunami Hazard. World Scientific Publishing Co., Singapore, pp. 308–324.
Fritz, H.M., Hager, W.H., Minor, H.E., 2001. Lituya Bay case: rockslide impact and wave run-up. Sci. Tsunami Hazards 19, 3–22.
Fritz, H.M., Hager, W.H., Minor, H.E., 2004. Near field characteristics of landslide generated impulse waves. J. Waterw. Port Coast. Ocean Eng. 130, 287–302.
Fukao, Y., 1973. Thrust faulting at a lithospheric plate boundary: the Portugal earthquake of 1969. Earth Planet. Sci. Lett. 18, 205–216.
Gan, W., Prescott, W.H., 2001. Crustal deformation rates in central and eastern U.S. inferred from GPS. Geophys. Res. Lett. 28, 3733–3736.
Geist, E.L., 1999. Local tsunamis and earthquake source parameters. Adv. Geophys. 39, 117–209.
Geist, E.L., 2002. Complex earthquake rupture and local tsunamis. J. Geophys. Res. 107. doi:10.1029/2000JB000139.
Geist, E.L., Parsons, T., 2006. Probabilistic analysis of tsunami hazards. Nat. Hazards 37, 277–314.
Geist, E.L., Parsons, T., 2008. Distribution of tsunami inter-event times. Geophys. Res. Lett. 35, L02612. doi:10.1029/2007GL032690.
Geist, E.L., Titov, V.V., Arcas, D., Pollitz, F.F., Bilek, S.L., 2007. Implications of the December 26, 2004 Sumatra–Andaman earthquake on tsunami forecast and assessment models for great subduction zone earthquakes. Bull. Seismol. Soc. Am. 97, S249–S270.
Geist, E.L., Lynett, P.J., Chaytor, J.D., 2009. Hydrodynamic modeling of tsunamis from the Currituck landslide. Mar. Geol. 264, 41–52 (this issue).
Geist, E.L., Parsons, T., ten Brink, U.S., Lee, H.J., 2009. Chapter 4: Tsunami Probability. In: E.N. Bernard and A.R. Robinson (Editors), The Sea, v. 15. Harvard University Press, Cambridge, Massachusetts.
Gisler, G., Weaver, R., Gittings, M.L., 2006. SAGE calculations of the tsunami threat from La Palma. Sci. Tsunami Hazards 24, 288–301.
Gjevik, B., et al., 1997. Modeling tsunamis from earthquake sources near Gorringe Bank southwest of Portugal. J. Geophys. Res. 102, 27,931–27,949.
Gràcia, E., Dañobeitia, J., Vergés, J., PARSIFAL Team, 2003. Mapping active faults offshore Portugal (36°N–38°N): implications for seismic hazard assessment along the southwest Iberian margin. Geology 31, 83–86.
Grilli, S.T., Watts, P., 2005. Tsunami generation by submarine mass failure. I: Modeling, experimental validation, and sensitivity analyses. J. Waterw. Port, Coastal, Ocean Eng. 131, 283–297.
Gutscher, M.-A., Baptista, M.A., Miranda, J.M., 2006. The Gibralter Arc seismogenic zone (part 2): constraints on a shallow east dipping fault plane source for the 1755 Lisbon earthquakes provided by tsunami modeling and seismic intensity. Tectonophysics 426, 153–166.
Guzzetti, F., Malamud, B.D., Turcotte, D.L., Reichenbach, P., 2002. Power–law correlations of landslide areas in central Italy. Earth Planet. Sci. Lett. 195, 169–183.
Harbitz, C.B., 1992. Model simulations of tsunamis generated by the Storegga slides. Mar. Geol. 105, 1–21.
Hartzell, S.H., Langer, C., Mendoza, C., 1994. Rupture histories of eastern North American earthquakes. Bull. Seismol. Soc. Am. 84, 1703–1724.
Hergarten, S., 2002. Self-Organized Criticality in Earth Systems. Springer, Berlin. 272 pp.
Hergarten, S., 2003. Landslides, sandpiles, and self-organized criticality. Nat. Hazards Earth Syst. Sci. 3, 505–514.
Hergarten, S., Neugebauer, H.J., 1998. Self-organized criticality in a landslide model. Geophys. Res. Lett. 25, 801–804.

Author's personal copy

Imamura, F., 2009. Chapter 10: Tsunami modeling: Calculating inundation and making hazard map. In: Robinson, A.R., Bernard, E.N. (Eds.), The Sea, v. 15. Harvard University Press, Cambridge, Massachusetts.
Imran, J., Parker, G., Locat, J., Lee, H., 2001. A 1-D numerical model of muddy subaqueous and subaerial debris flows. J. Hydraul. Eng. 127, 959-958.
Jibson, R.W., Harp, E.L., Michael, J.A., 2000. A method for producing digital probabilistic seismic landslide hazard maps. Eng. Geol. 58, 271–289.
Jiménez-Munt, I., Fernàndez, M., Torne, M., Bird, P., 2001. The transition from linear to diffuse plate boundary in the Azores–Gibraltar region: results from a thin-sheet model. Earth Planet. Sci. Lett. 192, 175–189.
Kafka, A.L., 2002. Statistical analysis of the hypothesis that seismicity delineates areas where future large earthquakes are likely to occur in the central and eastern United States. Seismol. Res. Lett. 73, 992–1003.
Kafka, A.L., Levin, S.Z., 2000. Does the spatial distribution of smaller earthquakes delineate areas where larger earthquakes are likely to occur? Bull. Seismol. Soc. Am. 90, 724–738.
Kagan, Y.Y., 1997. Seismic moment-frequency relation for shallow earthquakes: regional comparison. J. Geophys. Res. 102, 2835–2852.
Kagan, Y.Y., 2002. Seismic moment distribution revisited: I. statistical results. Geophys. J. Int. 148, 520–541.
Kagan, Y.Y., 2002. Seismic moment distribution revisited: II. moment conservation principle. Geophys. J. Int. 149, 731–754.
Kagan, Y.Y., Jackson, D.D., 1991. Seismic gap hypothesis: ten years after. Journal of Geophysical Research 96, 21,419–21,431.
Kagan, Y.Y., Jackson, D.D., 1995. New seismic gap hypothesis: five years after. J. Geophys. Res. 100, 3943–3959.
Kagan, Y.Y., Jackson, D.D., 2000. Probabilistic forecasting of earthquakes. Geophys. J. Int. 143, 438–453.
Kang, L.X., Wang, J.R., 1995. Episodes and ages of seismic landslides along the Changma fault zone. Acta Seismol. Sin. 8, 491–496.
Keefer, D.K., 1994. The importance of earthquake-induced landslides to long-term slope erosion and slope-failure hazards in seismically active regions. Geomorphology 10, 265–284.
Keefer, D.K., 2002. Investigating landslides caused by earthquakes—a historical review. Surv. Geophys. 23, 473–510.
Kijko, A., 2004. Estimation of the maximum earthquake magnitude, m_{max}. Pure Appl. Geophys. 161, 1655–1681.
Knight, W., 2006. Model predictions of Gulf and southern Atlantic coast tsunami impacts from a distribution of sources. Sci. Tsunami Hazards 24, 304–312.
Kreemer, C., Holt, W.E., Haines, A.J., 2002. The global moment rate distribution within plate boundary zones. In: Stein, S., Freymueller, J.T. (Eds.), Plate Boundary Zones. American Geophysical Union, Geodynamic Series, pp. 173–202. Washington, D.C.
Lee, H.J., 2005. Undersea landslides: extent and significance in the Pacific Ocean, an update. Nat. Hazards Earth Syst. Sci. 5, 877–892.
Lee, H.J., 2009. Timing of occurrence of large submarine landslides on the Atlantic ocean margin. Mar. Geol. 264, 53–64 (this issue).
Lee, E.M., Hall, J.W., Meadowcroft, I.C., 2001. Coastal cliff recession: the use of probabilistic prediction methods. Geomorphology 40, 253–269.
Liu, P.L.-F., 2009. Chapter 9: Tsunami modeling: propagation. In: Robinson, A.R., Bernard, E.N. (Eds.), The Sea, v. 15. Harvard University Press, Cambridge, Massachusetts.
Liu, P.L.F., Wu, T.-R., Raichlen, F., Synolakis, C.E., Borrero, J.C., 2005. Runup and rundown generated by three-dimensional sliding masses. J. Fluid Mech. 536, 107–144.
Locat, J., Lee, H.J., 2002. Submarine landslides: advances and challenges. Can. Geotech. J. 39, 193–212.
Locat, J., Lee, H.J., Locat, P., Imran, J., 2004. Numerical analysis of the mobility of the Palos Verdes debris avalanche, California, and its implication for the generation of tsunamis. Mar. Geol. 203, 269–280.
Locat, J., et al., 2009. Geomorphology, stability and mobility of the Currituck slide. Mar. Geol. 264, 28–40 (this issue).
Løvholt, F., Harbitz, C., Haugen, K.B., 2005. A parametric study of tsunami generated by submarine slides in the Ormen Lange/Storegga area off western Norway. Mar. Pet. Geol. 22, 219–231.
Lynett, P., Liu, P.L.F., 2002. A numerical study of submarine-landslide-generated waves and run-up. Proc. R. Soc. Lond., A 458, 2885–2910.
Mai, P.M., Beroza, G.C., 2000. Source scaling properties from finite-fault-rupture models. Bull. Seismol. Soc. Am. 90, 604–615.
Malamud, B.D., Turcotte, D.L., Guzzetti, F., Reichenbach, P., 2004. Landslide inventories and their statistical properties. Earth Surf. Proces. Landf. 29, 687–7111.
Maslin, M., Owen, M., Day, S., Long, D., 2004. Linking continental-slope failures and climate change: testing the clathrate gun hypothesis. Geology 32, 53–56.
Mazzotti, S., Adams, J., 2005. Rates and uncertainties on seismic moment and deformation in eastern Canada. J. Geophys. Res. 110. doi:10.1029/2004JB003510.
McCaffrey, R., 1994. Dependence of earthquake size distributions on convergence rates at subduction zones. Geophys. Res. Lett. 21, 2327–2330.
Mofjeld, H.O., González, F.I., Titov, V.V., Venturato, A.J., Newman, A.V., 2007. Effects of tides on maximum tsunami wave heights: probability distributions. J. Atmos. Ocean. Technol. 24, 117–123.
Murty, T.S., 2003. Tsunami wave height dependence on landslide volume. Pure Appl. Geophys. 1160, 2147–2153.
Nocquet, J.-M., Calais, E., 2004. Geodetic measurements of crustal deformation in the Western Mediterranean and Europe. Pure Appl. Geophys. (161), 661–681.
O'Loughlin, K.F., Lander, J.F., 2003. Caribbean tsunamis: a 500-year history from 1498–1998. Advances in Natural and Technological Hazards Research, 20. Kluwer Academic Publishers, Dordrecht, The Netherlands, p. 280.
Ogata, Y., 1999. Estimating the hazard of rupture using uncertain occurrence times of paleoearthquakes. J. Geophys. Res. 104, 17,995–18,014.
Okal, E.A., 1988. Seismic parameters controlling far-field tsunami amplitudes: a review. Nat. Hazards 1, 67–96.
Page, M.T., Carlson, J.M., 2006. Methodologies for earthquake hazard assessment: model uncertainty and the WGCEP-2002 forecast. Bull. Seismol. Soc. Am. 96, 1624–1633.
Parsons, T., 2002. Global Omori law decay of triggered earthquakes: large aftershocks outside the classical aftershock zone. J. Geophys. Res. 107, 2199. doi:10.1029/2001JB000646.
Parsons, T., 2008. Monte Carlo method for determining earthquake recurrence parameters from short paleoseismic catalogs: example calculations for California. J. Geophys. Res. 112. doi:10.1029/2007JB004998.
Parsons, T. Geist, E.L., in press. Tsunami probability in the Caribbean region. Pure and Applied Geophysics.
Pelayo, A.M., Wiens, D.A., 1992. Tsunami earthquakes: slow thrust-faulting events in the accretionary wedge. J. Geophys. Res. 97, 15,321–15,337.
Piper, D.J.W., Cochonat, P., Morrison, M.L., 1999. The sequence of events around the epicentre of the 1929 Grand Banks earthquake: initiation of debris flows and turbidity current inferred from sidescan sonar. Sedimentology 46, 79–97.
Rikitake, T., Aida, I., 1988. Tsunami hazard probability in Japan. Bull. Seismol. Soc. Am. 78, 1268–1278.
Rong, Y., Jackson, D.D., Kagan, Y.Y., 2003. Seismic gaps and earthquakes. J. Geophys. Res. 108, ESE 6–1–6-14.
Rossi, M. et al., 2007. Statistical and temporal properties of 596 triggered landslide events in the Emilia–Romagna region of Italy: 2007 European Geosciences Union General Assembly. Geophysical Research Abstracts, 9.
Senior Seismic Hazard Analysis Committee (SSHAC), 1997. Recommendations for Probabilistic Seismic Hazard Analysis: Guidance on Uncertainty and Use of Experts. NUREG/CR-6372 UCRL-ID-122160 Vol. 1, U.S. Nuclear Regulatory Commission, 256 pp.
Somerville, P.G., McLaren, J.P., LeFevre, L.V., Burger, R.W., Helmberger, D.V., 1987. Comparison of source scaling relations of eastern and western North American earthquakes. Bull. Seismol. Soc. Am. 77, 322–346.
Sornette, D., Sornette, A., 1999. General theory of the modified Gutenberg–Richter law for large seismic moments. Bull. Seismol. Soc. Am. 89, 1121–1130.
Stark, C.P., Hovius, N., 2001. The characterization of landslide size distributions. Geophys. Res. Lett. 28, 1091–1094.
ten Brink, U.S., Lin, J., 2004. Stress interaction between subduction earthquakes and forearc strike-slip faults: modeling and application to the northern Caribbean plate boundary. J. Geophys. Res. 109, B12310. doi:10.1029/2004JB003031.
ten Brink, U.S., Geist, E.L., Andrews, B.D., 2006. Size distribution of submarine landslides and its implication to tsunami hazard in Puerto Rico. Geophys. Res. Lett. 33. doi:10.1029/2006GL026125.
ten Brink, U.S., Lee, H.J., Geist, E.L., Twichell, D., 2009. Assessment of tsunami hazard to the U.S. Atlantic Coast using relationships between submarine landslides and earthquakes. Mar. Geol. 264, 65–73 (this issue).
Terrinha, P., et al., 2003. Tsunamigenic–seismogenic structures, neotectonics, sedimentary processes and slope instability on the southwest Portuguese Margin. Mar. Geol. 195, 55–73.
Thiebot, E., Gutscher, M.-A., 2006. The Gibraltar Arc seismogenic zone (part 1): constraints on a shallow east dipping fault plane source for the 1755 Lisbon earthquake provided by seismic data, gravity and thermal modeling. Tectonophysics 426, 135–152.
Titov, V.V., Mofjeld, H.O., González, F.I., Newman, J.C., 2001. Offshore forecasting of Alaskan tsunami in Hawaii. In: Hebenstreit, G.T. (Ed.), Tsunami Research at the End of a Critical Decade. Kluwer Academic Publishers, Dordrecht, The Netherlands, pp. 75–90.
Titov, V.V., Rabinovich, A.B., Mofjeld, H.O., Thomson, R., González, F.I., 2005. The global reach of the 26 December 2004 Sumatra tsunami. Science 309, 2045–2048.
Toro, G.R., Abrahamson, N.A., Schneider, J.F., 1997. Model of strong ground motions from earthquakes in central and eastern North America: best estimates and uncertainties. Seismol. Res. Lett. 68, 41–57.
Trauth, M.H., Bookhagen, B., Marwan, N., Strecker, M.R., 2003. Multiple landslide clusters record Quaternary climate changes in the northwestern Argentine Andes. Palaeogeogr. Palaeoclimatol. Palaeoecol. 194, 109–121.
Tsunami Pilot Study Working Group, 2006. Seaside, Oregon Tsunami Pilot Study—Modernization of FEMA Flood Hazard Maps, U.S. Geological Survey.
Vere-Jones, D., Robinson, R., Yang, W., 2001. Remarks on the accelerated moment release model: problems of model formulation, simulation and estimation. Geophys. J. Int. 144, 517–531.
Ward, S.N., 1980. Relationships of tsunami generation and an earthquake source. J. Phys. Earth 28, 441–474.
Ward, S.N., 1994. A multidisciplinary approach to seismic hazard in southern California. Bull. Seismol. Soc. Am. 84, 1293–1309.
Ward, S.N., 1997. More on M_{max}. Bull. Seismol. Soc. Am. 87, 1199–1208.
Ward, S.N., 2001. Landslide tsunami. J. Geophys. Res. 106, 11,201–11,215.
Wesnousky, S.G., 1994. The Gutenberg–Richter or characteristic earthquake distribution, which is it? Bull. Seismol. Soc. Am. 84, 1940–1959.
Wheeler, R.L., 1996. Earthquakes and the southeastern boundary of the intact Iapetan margin in eastern North America. Seismol. Res. Lett. 67, 77–83.
Wheeler, R.L., Frankel, A.D., 2000. Geology in the 1996 USGS seismic-hazard maps, central and eastern United States. Seismol. Res. Lett. 71, 273–282.
Wright, S.G., Rathje, E.M., 2003. Triggering mechanisms of slope instability and their relationship to earthquakes and tsunamis. Pure Appl. Geophys. 160, 1865–1877.
Wyss, M., 1979. Estimating maximum expectable magnitude of earthquake from fault dimensions. Geology 6, 336–340.
Yeh, H., 2009. Chapter 11: Tsunami impacts on coastlines. In: Robinson, A.R., Bernard, E.N. (Eds.), The Sea, v. 15. Harvard University Press, Cambridge, Massachusetts.
Zitellini, N., et al., 2004. Neogene through Quaternary tectonic reactivation of SW Iberian passive margin. Pure Appl. Geophys. 161, 565–587.